6054–6063 *Nucleic Acids Research, 2009, Vol. 37, No. 18* *Published online 21 August 2009*
doi:10.1093/nar/gkp684

Increased sister chromatid cohesion and DNA damage response factor localization at an enzyme-induced DNA double-strand break in vertebrate cells

Helen Dodson and Ciaran G. Morrison*

Centre for Chromosome Biology, School of Natural Sciences, National University of Ireland Galway, University road, Galway, Ireland

Received March 26, 2009; Revised July 29, 2009; Accepted August 3, 2009

ABSTRACT

The response to DNA damage in vertebrate cells involves successive recruitment of DNA signalling and repair factors. We used light microscopy to monitor the genetic dependencies of such localization to a single, induced DNA double strand break (DSB) in vertebrate cells. We used an inducible version of the rare-cutting I-SceI endonuclease to cut a chromosomally integrated I-SceI site beside a Tet operator array that was visualized by binding a Tet repressor-GFP fusion. Formation of γ-H2AX foci at a single DSB was independent of ATM or Ku70. ATM-deficient cells showed normal kinetics of 53Bp1 recruitment to DSBs, but Rad51 localization was retarded. 53Bp1 and Rad51 foci formation at a single DSB was greatly reduced in H2AX-null DT40 cells. We also observed decreased inter-sister chromatid distances after DSB induction, suggesting that cohesin loading at DSBs causes elevated sister chromatid cohesion. Loss of ATM reduced DSB-induced cohesion, consistent with cohesin being an ATM target in the DSB response. These data show that the same genetic pathways control how cells respond to single DSBs and to multiple lesions induced by whole-cell DNA damage.

INTRODUCTION

DNA double strand breaks (DSBs) are a particularly dangerous form of lesion that can arise during replication or be induced by ionizing radiation or radiomimetic chemicals. Failure to repair such damage accurately can lead to genome instability and cancer (1). To ensure that DSBs are repaired properly, vertebrate cells have evolved a complex and coordinated signalling network that detects damage, activates a transcriptional response and causes cell cycle delays during which DNA repair is initiated, with apoptosis as a possible outcome if the DNA damage is too great (2–4).

Current understanding of the DNA damage response to DSBs involves the activation of the ATM kinase through a mechanism involving its autophosphorylation and the Mre11/Nbs1/Rad50 complex (5). Active ATM causes the rapid phosphorylation of histone H2AX in large regions surrounding a DSB and the recruitment of additional factors to the break, including 53Bp1 and MDC1 (6–8). Recruitment of these elements of the DNA damage response is followed by the activation of checkpoint processes involving the Chk1 and Chk2 kinases and of DNA repair, involving the complementary activities of homologous recombination and non-homologous end-joining. An additional impact of DNA damage signalling is the recruitment of cohesin to extended regions around DSBs in yeast and human cells, with the suggestion that such local recruitment facilitates recombinational repair (9–11).

This successive localization of signalling and repair factors to a DSB has been described from the observation of foci induced by ionizing radiation (12,13), with further refinement coming from the use of masks to define the sites of damage (14). Laser microirradiation of small subnuclear tracts in sensitized live cells provided further insight into DNA damage response dynamics (15). Analysis of individual breaks involves the use of rare-cutting restriction endonucleases. This approach was pioneered in the study of recombinational repair by experiments involving the yeast HO endonuclease, which specifically recognizes the mating-type locus (16). Significant advances were made in the analysis of vertebrate homologous recombination by harnessing the yeast homing endonuclease, I-SceI (17,18). The recent combination of inducible endonucleases and the ability to detect repair factors localizing to the DSB by light microscopy or chromatin immunoprecipitation analysis (19,20) has

*To whom correspondence should be addressed. Tel: +353 91 49 20 56; Fax: +353 91 49 55 04; Email: ciaran.morrison@nuigalway.ie

allowed the examination of the DNA damage response at single DSBs. To determine whether single DSBs respond analogously to multiple DSBs, we introduced an inducible DSB system into chicken DT40 cells to probe the genetic dependencies of DNA damage response factor localization at a single DSB. We use a labelled chromosomal DSB to monitor how sister chromatid cohesion changes after DSB induction.

MATERIALS AND METHODS

Cloning

A 5.6-kb DNA fragment containing the repetitive tetracycline operator (TetO) array (x112) (21) was cloned into pBluescript. The restriction site for I-SceI was cloned in the BamH1 site of this vector at the end of the array using the following two oligos annealed together, 5′ GATCCTA GGGATAACAGGGTAATG 3′ and 5′ GATCCATTAC CCTGTTATCCCTAG 3′, yielding pTetO-I-SceI(RS). Tetracycline repressor cDNA (TetR) was cloned from p128TetR-GFP into pEGFP-N1 (Clontech) to create pTetR-GFP. The RFP-I-SceI-GR expression plasmid was received from Evi Soutoglou, NIH (20). To generate the *Ova*-targeting vector containing an I-SceI site we inserted the double-stranded oligonucleotide described above between the 5′ arm and the hygromycin resistance cassette of the targeting vector (22).

Cell culture and transfections

Wild type, $Ku70^{-/-}$ (23), $ATM^{-/-}$ (24) and $H2AX^{-/-}$ (25) clones of the chicken lymphoma B-cell line DT40 were cultured as described (23). DT40 stable cell lines with TetR-GFP-marked chromosomes were generated by co-transfection of pTetO-I-SceI(RS) and pTetR-GFP (23). Targeting of Atm was as previously described (24). Expression of RFP-I-SceI -GR in these cells was either by stable electroporation or transient nucleofection (Amaxa). RFP-I-SceI-GR expressing cells were cultured in RPMI supplemented with FCS and chicken serum (Lonza) which had been charcoal-stripped to remove any small molecules. Human U2OS cells were grown in DMEM supplemented with 10% charcoal-stripped FCS (Lonza). U2OS transfections were carried out using Lipofectamine 2000 (Invitrogen), and selected using G418 (0.4 mg/ml) for stable cell line generation. Nuclear localization of RFP-I-SceI-GR was achieved by adding triamcinolone acetonide (Sigma) to cells at a final concentration of 100 nM. For flow cytometrey cells were fixed in 70% ethanol then stained with propidium iodide (40 μg/ml) in PBS containing RNase A (100 μg/ml). Cell sorting was performed on a FACScalibur (BD Biosciences).

Ligation-mediated PCR

Genomic DNA (1 μg) was purified from DT40 cells with a stable TetO integration and TetR-GFP expression and ligated to an adaptor, made by annealing the following two oligonucleotides, 5′ GCATCACTACGATGTAG GATG 3′ and 5′ CATCCTACATCGTAGTGATGCT TAT 3′, at 16°C overnight. PCR was performed with a primer specific to the adaptor, 5′ CATCCTACATCGTA GTGATGC 3′ and one specific to the TetO array, 5′ GGA ACCGAGCCCGACTT 3′.

Immunoblotting

Whole cell extracts were prepared by lysis in 250 mM Tris–Cl, pH 7.5 with 0.1% Triton-X-100. Cell extracts were separated by SDS-PAGE and transferred to nitrocellulose. Samples were blotted with anti-phospho H2AX S139, clone JBW301 (Upstate), anti-phospho Chk1 S345 (Cell Signaling), anti-Rad51 (PC130; Oncogene), anti-actin (Sigma) and anti-tubulin clone B512 (Sigma).

Immunofluorescence microscopy

Cells were adhered to poly-L-lysine slides, fixation and antibody incubation was carried out as previously described (26). The following antibodies were used, anti-phospho H2AX S139, clone JBW301 (Upstate), 53BP1 (27) and Rad51 (PC130, Oncogene). For Rad51 cells were cytospun at 800 r.p.m. for 4 min prior to fixation. Cells were mounted using DABCO and imaging was performed using an Olympus BX51 microscope, ×100 objective, NA 1.35 using Openlab software (Improvision). Statistical analysis was performed using Prism v.5.0 (GraphPad).

RESULTS

Generation of an inducible DSB system in vertebrate cells

We aimed to generate a system for the visualization and analysis of single, chromosomal DSBs in vertebrate cells using the yeast homing endonuclease I-SceI. As shown in Figure 1A, we cloned the 18-bp recognition site for I-SceI beside a 112-repeat tetracycline operator array (TetO x112) (21) and co-transfected this construct into chicken DT40 and human U2OS cells along with an expression vector encoding a tetracycline repressor-GFP (TetR-GFP) fusion protein. We then selected for clones with either one or two GFP spots per cell, indicating TetR-GFP binding to the randomly integrated TetO array (data not shown). Genomic DNA from these clones was digested with various enzymes alone, or in combination with recombinant I-SceI, then Southern blotted and hybridized with the TetO array as probe (Figure 1B). We saw a decrease in the band sizes detected with the TetO array whenever recombinant I-SceI was added to a restriction digest (Figure 1B and data not shown), indicating that the I-Sce site was chromosomally integrated and accessible to restriction digestion. In a control experiment, we saw no decrease in the SacI band size after SacI-I-SceI double digestion, as the SacI site is located very close to the I-SceI site in the construct. A line diagram indicates the random integration of the TetO array into the genomic DNA, the probe used and the location of the SacI/PstI restriction sites external to the integrated construct (Figure 1B).

We first tried to induce DSBs in these clones using I-SceI fused to the ligand binding domain of the

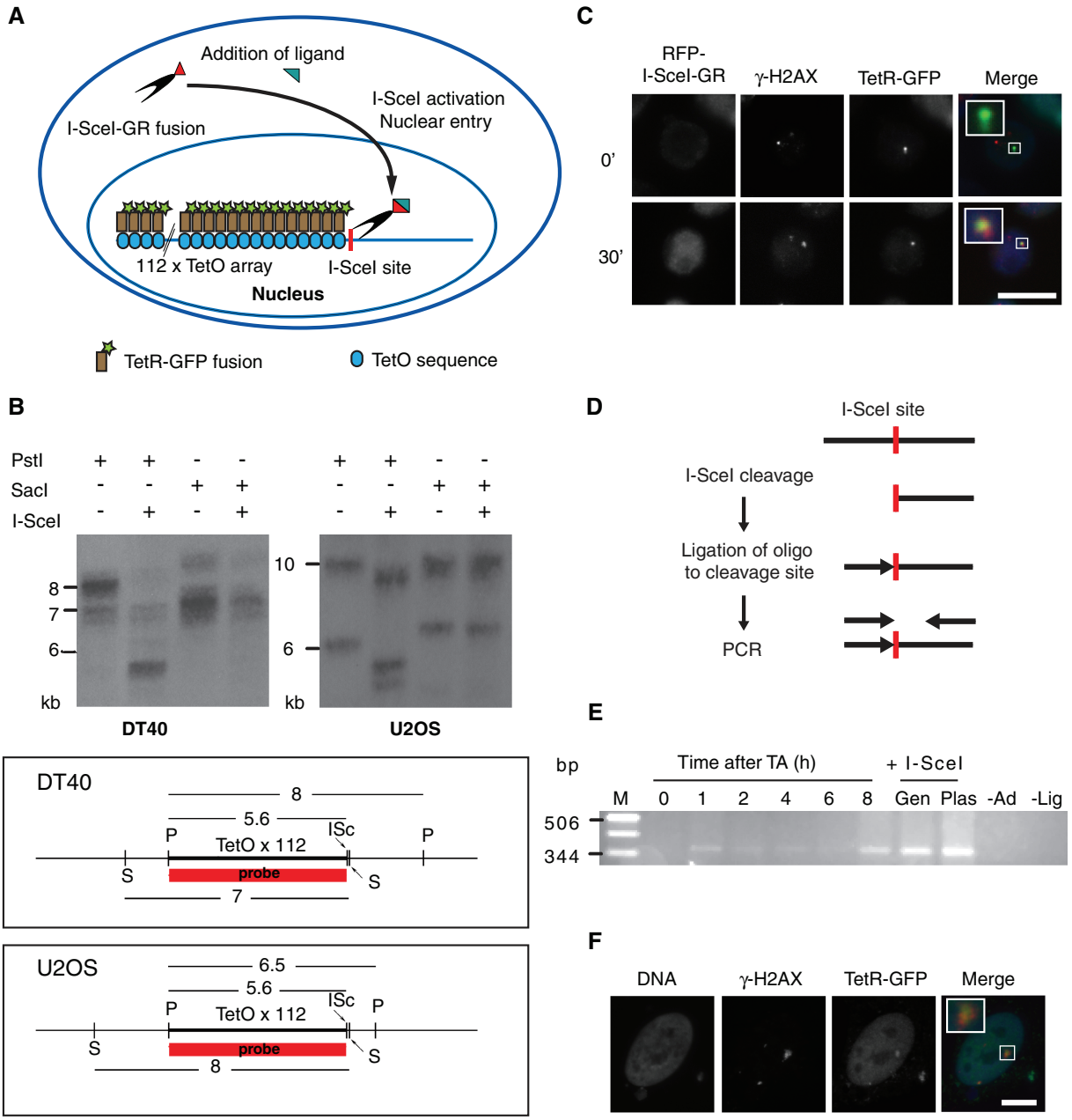

Figure 1. Generation of an inducible DSB in chicken DT40 cells and human U2OS cells. (**A**) Schematic representation of TetO/TetR array next to I-SceI restriction site. DSBs are induced by the addition of triamcinolone acetonide (TA), which results in the nuclear localization of the I-SceI endonuclease. (**B**) Southern blot analysis of *in vitro* I-SceI-digested genomic DNAs from DT40 and U2OS cells with randomly-integrated I-SceI sites, hybridized to the TetO array as probe. I-SceI cleaves within the genomic PstI fragments, but adjacent to the SacI site used in cloning the array. Line diagrams indicate the randomly integrated TetO array (TetO x112) and I-SceI restriction site (ISc) in the genomic DNA of both DT40 cells and U2OS cells. Locations for the SacI (S) and PstI (P) sites outside the integrated construct have been derived from the Southern blot data. The probe is shown in red. Numbers show fragment sizes in kilo basepairs. (**C**) Micrograph showing localization of RFP-I-SceI-GR (blue), γ-H2AX (red) and TetR-GFP (green) in DT40 cells, before and 30 min after addition of TA. Scale bar, 10 μm. (**D**) Diagram of the ligation-mediated PCR method used to detect a break following induction of I-SceI *in vivo*. (**E**) Ligation-mediated PCR. Genomic DNA was extracted from cells at the indicated time points following treatment with TA. Positive controls were genomic ('Gen') and plasmid ('Plas') DNA cut with recombinant I-SceI *in vitro*. Negative controls were genomic DNA cut with I-SceI *in vitro* in the absence of either the adaptor ('-Ad') or T4 DNA ligase ('-Lig'). (**F**) Micrograph showing localization of DNA (blue), γ-H2AX (red) and TetR-GFP (green) in a U2OS cell after transient transfection of an RFP-I-SceI-GR expression construct. Scale bar, 10 μm.

estrogen receptor (ER), expecting rapid nuclear localization of the I-SceI-ER fusion protein in response to 4-hydroxytamoxifen (4-OHT). However, we did not see any induction of DSBs with this approach. We then turned to a fusion between I-SceI and the glucocorticoid receptor (GR), which can be activated by addition of triamcinolone acetonide (TA) (20). We used red fluorescent protein (RFP) fused to I-SceI-GR to identify cells that expressed the endonuclease (20).

Before or 30 min after addition of the activating TA, DT40 cells were fixed and stained with an antibody to the DNA damage response marker, γ-H2AX, then

visualized using microscopy. As shown in Figure 1C, the RFP-I-SceI-GR moved to the nucleus after TA activation. We saw co-localization of γ-H2AX with the TetR-GFP-marked array, indicating the formation of DSBs. To confirm the generation of these breaks, we used ligation-mediated PCR. Genomic DNA was extracted from DT40 cells with an integrated TetO array and expressing both TetR-GFP and RFP-I-SceI-GR. Cells had either been untreated or treated for various times with TA. A double-stranded oligonucleotide with an overhang specific for the I-SceI cut site was ligated to the genomic DNA and primers specific for the ligated oligonucleotide and the TetO array were used for PCR amplification (Figure 1D). As shown in Figure 1E, the diagnostic 360 bp band was amplified from genomic DNA after I-SceI induction *in vivo* or after *in vitro* I-SceI digestion. A positive control for the ligation-mediated PCR was the amplification of *in vitro* I-SceI-digested plasmid DNA. Notably, no amplification was seen in the absence of TA or in the absence of either the double stranded adaptor or T4 DNA ligase, confirming the specificity of the reaction and the reliability of the TA induction of the I-SceI.

This DSB induction system was also successfully introduced into U2OS cells. In a manner similar to that described for the DT40 cells we determined that the I-SceI sites was chromosomally integrated and accessible to restriction digestion by digestion of genomic DNA and Southern blotting (Figure 1B). We confirmed the chromosomal integration of the TetO array and binding of the TetR-GFP protein by microscopy (Figure 1F). This cell line was then transiently transfected with the RFP-I-SceI-GR construct and treated with TA. Although Southern analysis did not demonstrate cleavage at the I-SceI site *in vivo* (data not shown), microscopy showed the colocalization of γ-H2AX with the TetR-GFP-marked array (Figure 1F and Supplementary Figure 2), confirming DSB induction.

Analysis of I-SceI digestion of a site integrated at the DT40 *Ovalbumin* locus

We wished to use Southern blot to monitor I-SceI activity, so we exploited the high frequency of gene targeting seen in DT40 cells to integrate an I-SceI restriction site at a known chromosomal location, namely the *Ovalbumin* (*Ova*) locus (22). Wild-type and non-homologous end-joining-deficient $Ku70^{-/-}$ cells were transfected with a hygromycin-containing *Ova* targeting vector that carried an I-SceI site without the TetO array. Clones were selected and screened for integration at the locus by Southern blot. As shown in the supplemental information (Supplementary Figure 1A), *Ova* was targeted in both the wild type and $Ku70^{-/-}$ cells, and the integrated I-SceI site was cut *in vitro* by recombinant I-SceI. These cells were then stably transfected with RFP-I-SceI-GR, screened for expression of RFP and tested for the induction of a DSB at the *Ova* locus (Supplementary Figure 1B). We detected no cutting at *Ova* by Southern blot following the addition of TA in 10 I-SceI-GR-expressing wild-type and 6 $Ku70^{-/-}$ clones, leading us to conclude that the efficiency of any *in vivo* I-SceI cleavage at the *Ova* locus was too low to analyse by Southern blot.

Involvement of *H2AX*, *ATM* and *Ku70* in γ-H2AX and 53Bp1 localization to I-SceI -induced DSBs

We used microscopy to monitor the timing and frequency of colocalization of γ-H2AX and the TetO array as an indicator of DSB induction after I-SceI activation in DT40 cells (Figures 1C and 2A). We observed a time-dependent increase in the percentage of RFP-I-SceI-GR-positive cells that showed a co-localization between the γH2AX and the TetO array following the addition of the drug TA (Figure 2B), with around 60% of cells having a DSB 4–6 h after induction. Higher levels of induction were reported in a similar experiment performed in mouse cells (20), where 80% of cells showed localization of γ-H2AX foci to a target array 30 min after drug addition. We do not have an explanation for this difference, which may relate to I-SceI expression levels or cell type- or species-specificity. We confirmed these microscopy data by immunoblot analysis of γ-H2AX induction (Figure 2C). As Chk1 is phosphorylated following IR treatment through a mechanism involving ATM recruitment of ATR to DSBs and subsequent Chk1 activation (28,29), we also examined the levels of phospho-Chk1 to monitor the extent of checkpoint activation and found no major increase in Chk1 phosphorylation (Figure 2C). We then used flow cytometry to test whether the DNA damage response impacted on the cell cycle. No difference in the cell cycle profile as determined by DNA labelling was observed following addition of TA (Figure 2D). We also monitored the G2 checkpoint after I-SceI induction by culturing cells in nocodazole and measuring the increase in mitotic index over 4 h. No difference in the mitotic percentages was observed in the presence or absence of TA (data not shown). These results suggest that an I-SceI-induced break at one locus did not cause significant checkpoint activation, as determined by phosphorylation of Chk1 or a G2 phase cell cycle arrest.

To test whether the response to I-SceI-induced DSBs involves the ATM kinase or the non-homologous end-joining (NHEJ) pathway of DNA repair, we analysed the kinetics of γ-H2AX localization to the TetO array after I-SceI induction in $Atm^{-/-}$ and $Ku70^{-/-}$ DT40 cells. As shown in Figure 2B, the kinetics of γH2AX/TetO array colocalization was very similar for wild type, ATM mutant and Ku70 mutant cells, indicating that neither ATM signalling nor NHEJ are required for the generation of the γ-H2AX signal seen after I-SceI digestion of chromosomal DNA. To analyse H2AX-dependent activities in response to enzymatic DSB induction, we also integrated this DSB system into $H2ax^{-/-}$ DT40 cells (25). Following transient transfection of RFP-I-SceI-GR in $Atm^{-/-}$ and $H2ax^{-/-}$ mutant cells we followed the colocalization of the TetO array with the DNA damage response factor 53Bp1 (Figure 3A). The kinetics of 53Bp1 localization to the induced DSB were very similar in $Atm^{-/-}$ cells and in wild-type cells that stably expressed the RFP-I-SceI-GR, and closely reflected the kinetics of

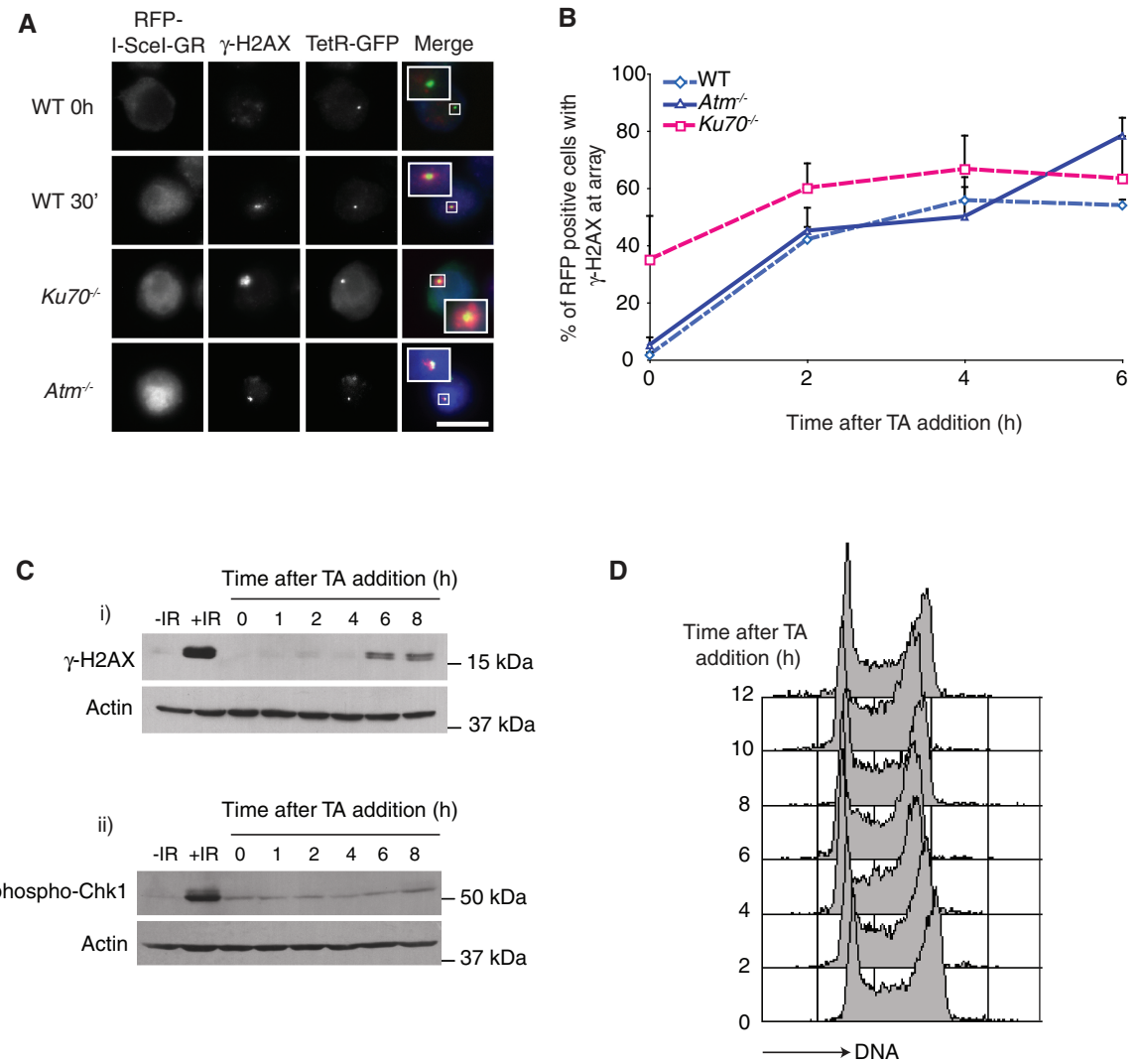

Figure 2. γ-H2AX recruitment to the TetO array after I-SceI induction. (**A**) Micrograph showing localization of RFP-I-SceI-GR (blue), γ-H2AX (red) and TetR-GFP (green) in DT40 cells of the indicated genotype, before and 30 min after addition of TA. Scale bar, 10 μm. (**B**) Graph showing the kinetics of γ-H2AX localization at the array in wild type, *Ku70*$^{-/-}$ and *Atm*$^{-/-}$ DT40 cells. At least 20 cells that stably expressed RFP-I-SceI-GR, as determined by microscopy, were analysed per timepoint for each cell line. The experiment was repeated at least three times for each cell line and the error bars show the SEM. (**C**) Immunoblot showing (i) γ-H2AX levels, and (ii) Chk1 levels in wild-type I-SceI site-containing cells that stably express RFP-I-SceI-GR over time following TA addition. Wild-type DT40 cells treated with 20 Gy IR 1 h before harvesting were used as positive control. Actin was used as a loading control. (**D**) Flow cytometry analysis of I-SceI site-containing wild-type cells that stably express RFP-I-SceI-GR at the indicated times after induction of I-SceI.

γ-H2AX localization. However, in H2AX-deficient cells, only a very small percentage showed co-localization between 53Bp1 and the array (Figure 3B). This suggests that efficient 53Bp1 localization to I-SceI-induced DSBs requires H2AX.

Genetic dependencies of Rad51 localization to I-SceI -induced DSBs

To determine the relationship between DNA damage signalling and DNA repair of the I-SceI-induced DSB, we examined the colocalization of the Rad51 recombinase with the TetO array (Figure 4A). The kinetics of localization of both γ-H2AX and Rad51 to the array in wild type cells were very similar, both peaking at 4 h after the addition of TA (Figure 4B). The percentage of γ-H2AX positive cells that also had Rad51 at the array was recorded. This was maximal at 2 h after TA addition, consistent with the recruitment of Rad51 to γ-H2AX-containing chromatin (30). We then investigated the localization of Rad51 at the array in *H2ax*$^{-/-}$ and *Atm*$^{-/-}$ DT40 cells. These mutant lines were transiently transfected with RFP-I-SceI-GR and then the percentage of cells showing colocalization between the array and Rad51 was recorded (Figure 4C). Rad51 localization to the induced DSB was slow and inefficient in both ATM- and H2AX-deficient cells (Figure 4D). Immunoblot analysis demonstrated that Rad51 protein levels were not affected by the loss of either ATM or H2AX (Figure 4E). These data indicate defective Rad51 mobilization to a single enzyme-induced DSB, consistent with

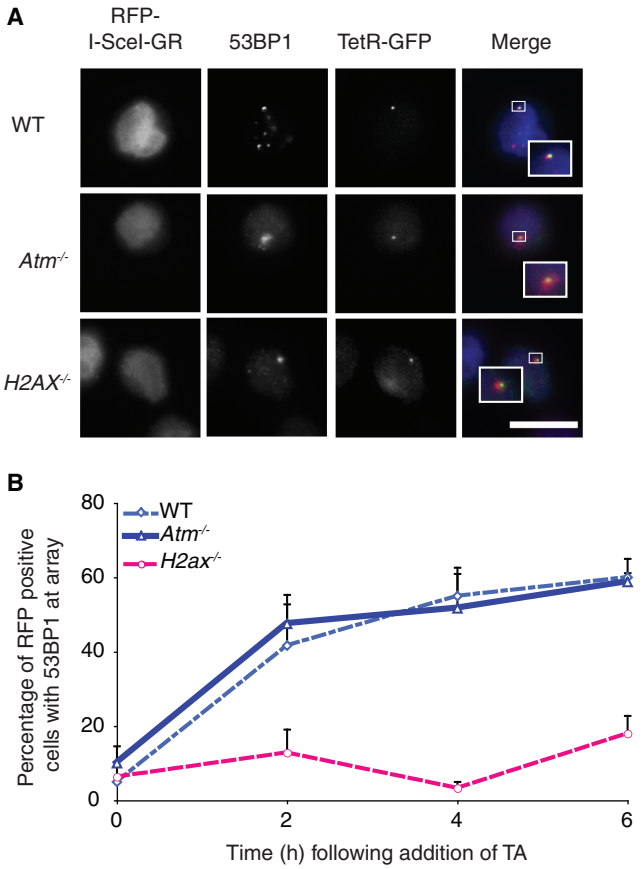

Figure 3. Abnormal recruitment of 53Bp1 to DSBs in $H2AX^{-/-}$ cells. (**A**) Micrograph showing localization of RFP-I-SceI-GR (blue), 53Bp1 (red) and TetR-GFP (green) in DT40 cells after addition of TA. WT cells were stably transfected with an RFP-I-SceI-GR expression vector and treated with TA for 2 h. $Atm^{-/-}$ and $H2ax^{-/-}$ cells were transiently transfected with the RFP-I-SceI-GR expression construct and 16 h post-transfection, treated with TA for 4 and 6 h, respectively. Scale bar, 10 μm. (**B**) Graph showing the kinetics of 53Bp1 localization at the array in RFP-I-SceI-GR-expressing DT40 cells of the indicated genotypes. At least 20 cells that expressed RFP-I-SceI-GR, as determined by microscopy, were analysed per timepoint for each cell line. The experiment was repeated at least three times for each cell line and the error bars show the SEM.

previous observations of defective IR-induced Rad51 focus formation in $Atm^{-/-}$ and $H2ax^{-/-}$ cells (24,25).

Impact of DSBs on sister chromosome proximity

Several recent studies in yeast and vertebrate cells have shown a connection between the cohesin complex and DSB repair (31,32). Cohesin is recruited around DSBs in yeast (10,11,33,34) and human cells (9). To test whether such recruitment could impact on sister chromatid cohesion, we induced a single DSB in DT40 cells using the inducible I-SceI system and measured the distances between the TetR-GFP spots on opposite sister chromatids in mitotic cells. We used γ-H2AX localization to the array to determine whether a DSB had been generated in a given cell (Figure 5A). Mitotic cells were analysed to ensure that two sisters were visible, as very close TetO arrays in G2 cells might have been scored as single foci in G1. Recent data have indicated that low-levels of DSB induction by IR do not arrest cells in G2 (35). Cells from the same experiment but without γ-H2AX at the TetO sites were used as a negative control and showed no difference in inter-sister distances from untreated cells (Figure 5B). We found that inter-sister distances were significantly reduced where a DSB was induced (Figure 5B), suggesting that one outcome of DSB-induced cohesin loading is an increased proximity of sister chromatids.

We next wished to test whether this cohesion involved the cohesin complex. The tet-repressible *Scc1* transgene precluded our using the conditional *Scc1* knockout DT40 line (31), so we attempted to use RNAi of cohesin in the U2OS cell line. Unfortunately, in U2OS cells colocalization of the γ-H2AX signal with the TetO array was not visible above the high background in transfected mitotic cells (Supplementary Figure 2). However, recent data have indicated that the cohesin complex is an ATM target in the DNA damage response (36–38) so next, we tested whether the DSB signal through ATM mediates increased sister chromatid cohesion. We targeted the *Atm* locus in the same TetO-integrated, inducible I-SceI and TetR-GFP-expressing clone used for the cohesion analysis (Figure 6A). Inducible I-SceI expression and DSB induction was maintained in $Atm^{-/-}$ clones (Figure 6B). When we measured the inter-sister distances, we found that they were indistinguishable between wild-type and $Atm^{-/-}$ cells, but that the reduction in sister separation after DSB induction was significantly greater in wild-type than in $Atm^{-/-}$ cells (Figure 6C). This observation suggests that the increased cohesion at a DSB involves ATM activity.

DISCUSSION

Here we show that an RFP-I-SceI-GR fusion can be activated to generate DSBs adjacent to a chromosomally integrated TetO array in chicken DT40 and human U2OS cells, as has been successfully demonstrated in mouse cells (20). We used Southern analysis after *in vitro* I-SceI digestion to confirm that the restriction site beside the TetO array could be cleaved and then used ligation-mediated PCR to demonstrate the inducible activity of I-SceI-GR *in vivo*. Southern blotting did not detect I-SceI cleavage at either randomly-integrated or gene-targeted (*Ova*) sites after induction of the recombinant enzyme in cells, indicating that the I-SceI sites are cut with relatively low efficiency in the entire population. This is consistent with previous work using transient transfection of I-SceI-expressing vectors, where cleavage-induced recombination occurs in a relatively small fraction of the total cell number transfected (17). However, when we limited our analysis to cells that expressed I-SceI, as detected by the RFP tag, we found a robust level of DSB induction and monitored the localization of repair factors at the induced break site, using microscopy. Alternatively, the cleavage may be repaired very efficiently, rendering the cut undetectable. A site repaired by homologous recombination is likely to be re-cut by the enzyme. However, if the

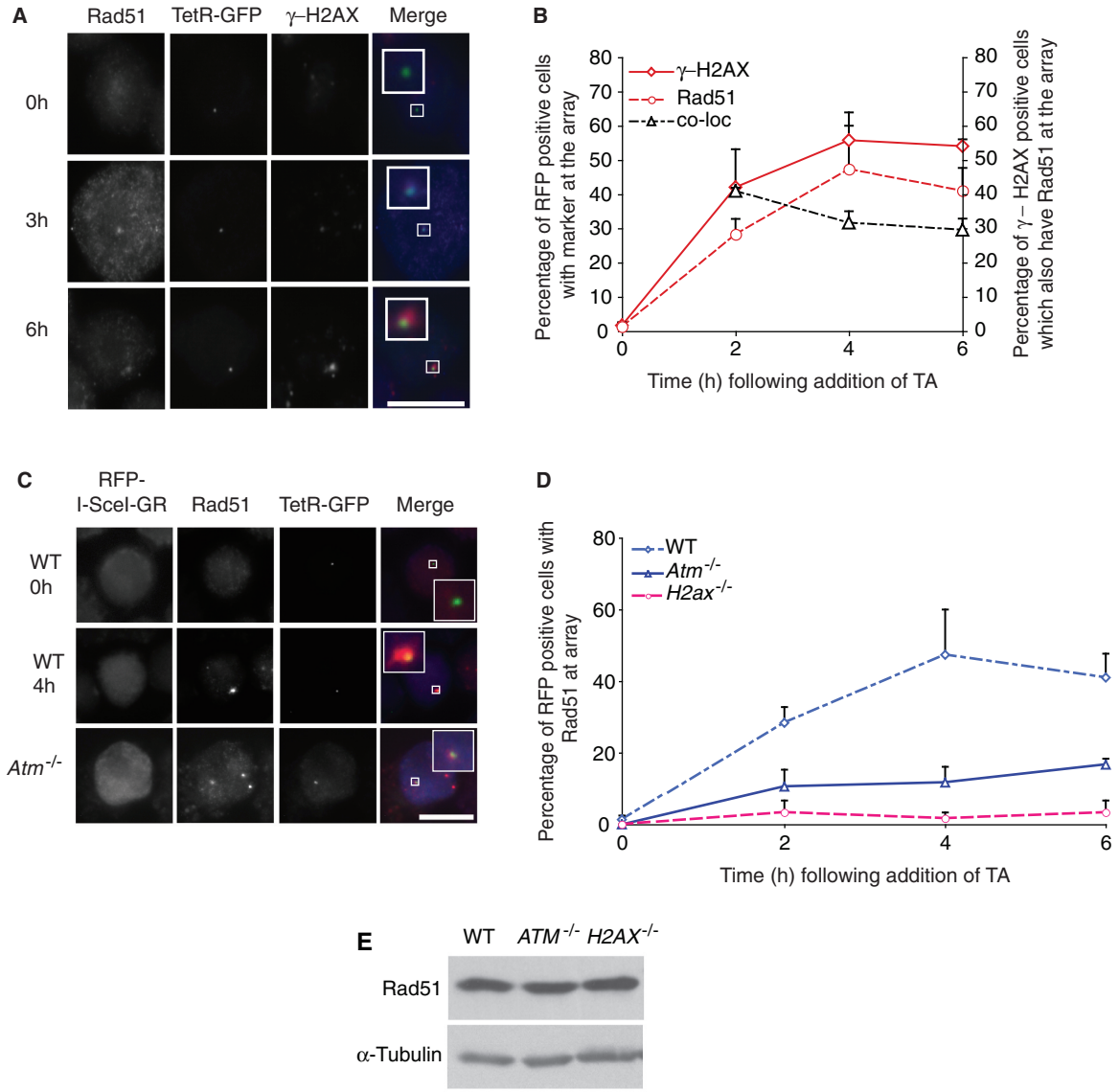

Figure 4. Abnormal recruitment of Rad51 to DSBs in $H2AX^{-/-}$ and $ATM^{-/-}$ cells. (**A**) Micrograph showing localization of γ-H2AX (red), Rad51 (blue) and TetR-GFP (green) in DT40 cells, before and at the indicated times after addition of TA. Scale bar, 10 μm. (**B**) Graph comparing the kinetics of γ-H2AX and Rad51 recruitment to the array in wild type cells that stably express RFP-I-SceI-GR over time following TA addition. At least 20 cells per timepoint were scored for localization of γ-H2AX, Rad51 (red curves, left axis) or both (the percentage of γ-H2AX/array positive cells which also have Rad51; black curve, right axis) at the array. The experiment was repeated at least three times and the error bars show the SEM. (**C**) Micrograph showing localization of RFP-I-SceI-GR (blue), Rad51 (red) and TetR-GFP (green) in wild-type and $Atm^{-/-}$ DT40 cells, before and at the indicated times after addition of TA. WT cells were stably transfected with an RFP-I-SceI-GR expression vector and treated with TA for 4 h. $Atm^{-/-}$ cells were transiently transfected and 16 h post-transfection, treated with TA for 2 h. Scale bar, 10 μm. (**D**) Graph showing the kinetics of Rad51 localization at the array in RFP-I-SceI-GR-positive $Atm^{-/-}$ and $H2ax^{-/-}$ DT40 cells after transient transfection with RFP-I-SceI-GR. At least 20 cells that expressed RFP-I-SceI-GR, as determined by microscopy, were analysed per timepoint for each cell line. The experiment was repeated at least three times for each cell line and the error bars show the SEM. (**E**) Immunoblot showing the Rad51 levels in wild-type, $Atm^{-/-}$ and $H2ax^{-/-}$ cells. α-tubulin was used as a loading control.

cut is repaired by an error-prone process, such as NHEJ, it seems unlikely that the site would remain intact. By analysing digestion at *Ova* in $Ku70^{-/-}$ cells, we expected to have forced the repair to involve homologous recombination and thus result in high levels of re-cleavage. However, no difference in the efficiency of cutting was detected, emphasizing a low level of cleavage in the entire population after I-SceI induction. These observations suggest that the ability of I-SceI to find its cognate site repeatedly is relatively low.

We then used microscopy to characterize the formation of DNA damage response foci after DSB induction. While DSB induction by ionizing irradiation causes rapid γ-H2AX focus formation (30,39), the percentage of DT40 cells with γ-H2AX foci at the TetO array increased until 4 h post-induction, suggesting that I-SceI digestion is not synchronous in the entire population. These kinetics were slower than those observed in NIH3T3 cells with the same I-SceI expression construct, where maximal focus formation at an induced lesion

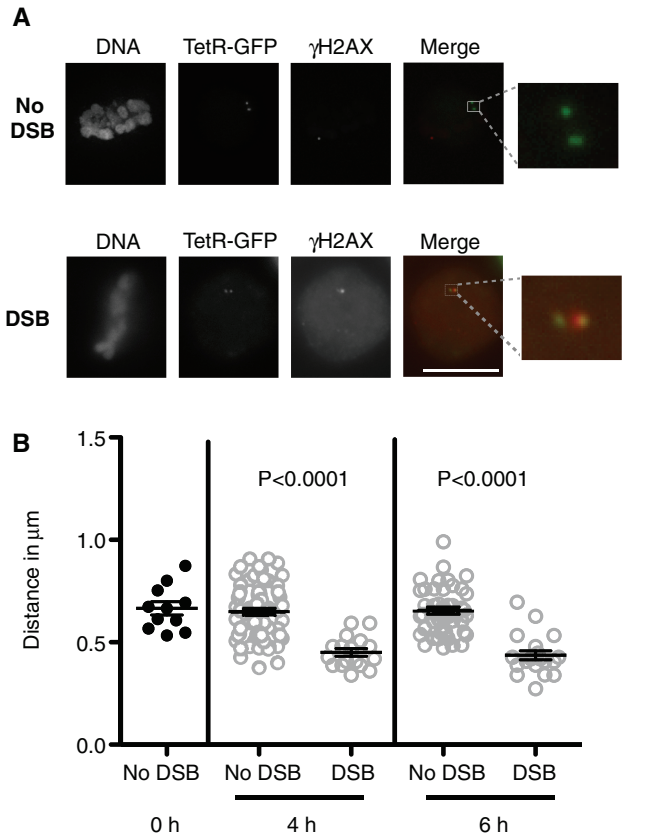

Figure 5. Decreased inter-sister chromatid distances at DSB sites. (**A**) DT40 cells were fixed and stained with antibodies to γ-H2AX (red) and counterstained with DAPI following addition of TA. The distance between GFP spots (green), which mark the TetO array, was measured in metaphase mitotic chromosomes. The presence of a γ-H2AX signal at the TetO array indicated a DSB site. Scale bar, 10 μm. (**B**) Analysis of distances between GFP spots. Pooled data from three independent repeats of the experiment are shown as individual data points and as mean ± SEM. At each timepoint, inter-sister distances were significantly reduced in cells with a DSB ($P < 0.0001$, unpaired Student's *t*-test).

occurred 30 min after induction (20). We attribute this difference to a variation in I-SceI cutting of the different sites or to differing expression levels of I-SceI in transient versus stable expression experiments, as the enzyme rapidly relocates to the nucleus after TA addition to DT40 cell cultures. The kinetics of 53Bp1 foci formation at the TetO array closely followed those of γ-H2AX, as was expected from the previously-described responses of 53Bp1 to DSBs induced by IR and I-SceI (20,27). The localization of the Rad51 recombinase to the DSB occurred slightly after the formation of γ-H2AX foci, which agrees with the successive recruitment of signalling and repair factors to IR-induced lesions (14,30). Despite the effective induction of a DNA damage response in terms of DSB-localizing foci, we saw no G2-M checkpoint delay. This is consistent with there being a threshold of >10 breaks/cell for G2-M arrest, as was proposed to explain the absence of a G2-M arrest in human fibroblasts after low-level DSB induction by IR (35).

We then examined the genetic dependencies of the focus formation at induced I-SceI breaks in DT40 cells. γ-H2AX foci formed in $Atm^{-/-}$ and $Ku70^{-/-}$ cells with kinetics indistinguishable from those of wild-type cells, demonstrating that neither of these genes is required for H2AX phosphorylation at I-SceI sites. These data support the redundant functioning of ATM and DNA-PK in γ-H2AX focus formation after enzymatic DSB induction (40), rather than a requirement for ATM (41). ATM deficiency retarded Rad51 focus formation at the I-SceI break, as has already been noted for IR-induced foci (24). The loss of H2AX greatly reduced 53Bp1 localization to the TetO array, consistent with the previously-described poor retention of 53Bp1 at IR- or laser-scissors-induced DSBs in H2AX-deficient mouse cells (42,43). Notably, efficient Rad51 focus formation at the I-SceI site after induction required H2AX. This is consistent with the defective ionizing radiation-induced Rad51 foci formation in $H2ax^{-/-}$ DT40 cells (25), which was not seen in *H2AX* null mouse cells (43).

Having established a system by which we could monitor DSBs by microscopy, we tested whether the increased cohesin reported at DSBs impacted on sister chromatid cohesion (9–11,33,34). Our results clearly showed decreased inter-sister distances in mitosis after DSB induction. These data reveal that DSBs induce increased sister chromatid cohesion, indicating a functional consequence of cohesin loading that may facilitate recombinational repair, as has been suggested from studies of cohesin-deficient yeast and vertebrate cells (31,32). Notably, the loss of ATM reduced the extent to which DSB induction caused increased sister chromatid cohesion. As both Smc1 and Scc1 (Mcd1) are cohesin targets of the DNA damage response (36–38), it is conceivable that the ATM- or Chk1-dependent phosphorylation of Smc1 and/or Scc1 results in increased cohesion at a DSB, although the mechanism by which such phosphorylation-induced cohesion arises is unknown. An alternative possibility is that the ATM-dependent recombinational repair activity at induced DSBs mediates increased sister chromatid proximity. We were unable to repress sufficiently Smc1 or Scc1 in our system to distinguish directly between these hypotheses.

Together, our data indicate that I-SceI induces DSBs in chicken DT40 cells. These DSBs are recognized by the DNA damage response apparatus in a manner that reflects the response to multiple non-enzymatic breaks, such as those induced by IR. This system also allows the analysis of break-induced cohesion and has suggested a role for the DNA damage response in controlling sister chromatid cohesion.

SUPPLEMENTARY DATA

Supplementary Data are available at NAR Online.

ACKNOWLEDGEMENTS

The authors thank Tomoyuki Tanaka, Evi Soutoglou and Tom Misteli for plasmid constructs, Thanos Halazonetis

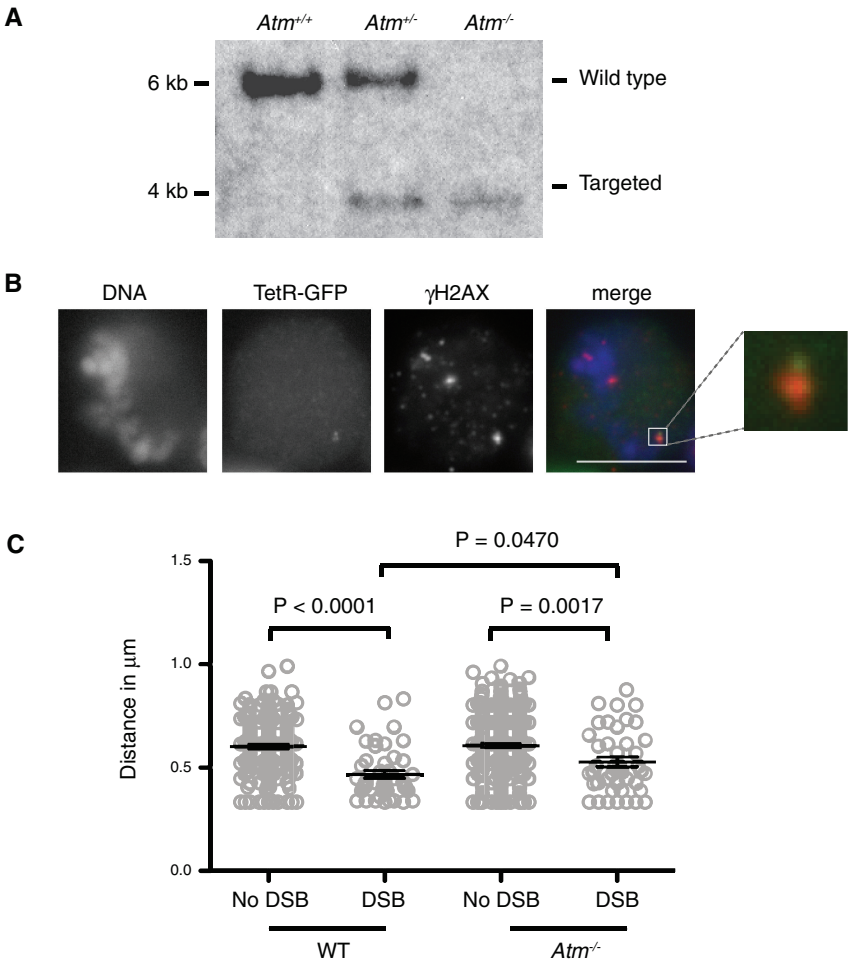

Figure 6. Involvement of ATM in inter-sister chromatid distances at DSB sites. (**A**) Southern blot showing the targeting of *Atm* in the same clone used for the analysis in Figure 5. (**B**) DT40 cells were fixed and stained with antibodies to γ-H2AX (red) and counterstained with DAPI following addition of TA. The distance between GFP spots (green), which mark the TetO array, was measured in metaphase mitotic chromosomes. The presence of a γ-H2AX signal at the TetO array indicated a DSB site. Scale bar, 10 µm. (**C**) Analysis of distances between GFP spots. Pooled data from three independent repeats of the experiment are shown as individual data points and as mean ± SEM. Comparison of the mean distances using an unpaired Student's *t*-test showed no difference between wild-type and $Atm^{-/-}$ sister chromatid separation in the absence of DNA damage (data not shown), a highly-significant reduction in inter-sister distances in wild-type chromatids with a DSB ($P < 0.0001$) and a notably less significant reduction in inter-sister distances in $Atm^{-/-}$ chromatids after DSB induction ($P = 0.0017$). The inter-sister chromatid separation after DSB induction differed between wild-type and $Atm^{-/-}$ cells with a moderate level of statistical significance ($P = 0.0470$).

for antibodies and Shunichi Takeda for cell lines, as well as James Brown, Noel Lowndes and Stephen Rea for comments on the manuscript.

FUNDING

Science Foundation Ireland grants (05/RFP/Gen0034; 08/IN.1/B1029). Funding for open access charge: Science Foundation Ireland principal investigator grant.

Conflict of interest statement. None declared.

REFERENCES

1. Khanna,K.K. and Jackson,S.P. (2001) DNA double-strand breaks: signaling, repair and the cancer connection. *Nat. Genet.*, **27**, 247–254.
2. Jackson,S.P. (2002) Sensing and repairing DNA double-strand breaks. *Carcinogenesis*, **23**, 687–696.
3. Shiloh,Y. (2003) ATM and related protein kinases: safeguarding genome integrity. *Nat. Rev. Cancer*, **3**, 155–168.
4. Zhou,B.B. and Elledge,S.J. (2000) The DNA damage response: putting checkpoints in perspective. *Nature*, **408**, 433–439.
5. Lavin,M.F. (2007) ATM and the Mre11 complex combine to recognize and signal DNA double-strand breaks. *Oncogene*, **26**, 7749–7758.
6. DiTullio,R.A. Jr, Mochan,T.A., Venere,M., Bartkova,J., Sehested,M., Bartek,J. and Halazonetis,T.D. (2002) 53BP1 functions in an ATM-dependent checkpoint pathway that is constitutively activated in human cancer. *Nat. Cell Biol.*, **4**, 998–1002.
7. Rogakou,E.P., Boon,C., Redon,C. and Bonner,W.M. (1999) Megabase chromatin domains involved in DNA double-strand breaks in vivo. *J. Cell Biol.*, **146**, 905–916.
8. Stucki,M., Clapperton,J.A., Mohammad,D., Yaffe,M.B., Smerdon,S.J. and Jackson,S.P. (2005) MDC1 directly binds phosphorylated histone H2AX to regulate cellular responses to DNA double-strand breaks. *Cell*, **123**, 1213–1226.
9. Kim,J.S., Krasieva,T.B., LaMorte,V., Taylor,A.M. and Yokomori,K. (2002) Specific recruitment of human cohesin to laser-induced DNA damage. *J. Biol. Chem.*, **277**, 45149–45153.
10. Strom,L., Lindroos,H.B., Shirahige,K. and Sjogren,C. (2004) Postreplicative recruitment of cohesin to double-strand breaks is required for DNA repair. *Mol. Cell*, **16**, 1003–1015.

11. Unal,E., Arbel-Eden,A., Sattler,U., Shroff,R., Lichten,M., Haber,J.E. and Koshland,D. (2004) DNA damage response pathway uses histone modification to assemble a double-strand break-specific cohesin domain. *Mol. Cell*, **16**, 991–1002.
12. Haaf,T., Golub,E.I., Reddy,G., Radding,C.M. and Ward,D.C. (1995) Nuclear foci of mammalian Rad51 recombination protein in somatic cells after DNA damage and its localization in synaptonemal complexes. *Proc. Natl Acad. Sci. USA*, **92**, 2298–2302.
13. Maser,R.S., Monsen,K.J., Nelms,B.E. and Petrini,J.H. (1997) hMre11 and hRad50 nuclear foci are induced during the normal cellular response to DNA double-strand breaks. *Mol. Cell Biol.*, **17**, 6087–6096.
14. Nelms,B.E., Maser,R.S., MacKay,J.F., Lagally,M.G. and Petrini,J.H. (1998) In situ visualization of DNA double-strand break repair in human fibroblasts. *Science*, **280**, 590–592.
15. Lukas,C., Falck,J., Bartkova,J., Bartek,J. and Lukas,J. (2003) Distinct spatiotemporal dynamics of mammalian checkpoint regulators induced by DNA damage. *Nat. Cell Biol.*, **5**, 255–260.
16. Paques,F. and Haber,J.E. (1999) Multiple pathways of recombination induced by double-strand breaks in Saccharomyces cerevisiae. *Microbiol. Mol. Biol. Rev.*, **63**, 349–404.
17. Richardson,C., Moynahan,M.E. and Jasin,M. (1998) Double-strand break repair by interchromosomal recombination: suppression of chromosomal translocations. *Genes Dev.*, **12**, 3831–3842.
18. Rodrigue,A., Lafrance,M., Gauthier,M.C., McDonald,D., Hendzel,M., West,S.C., Jasin,M. and Masson,J.Y. (2006) Interplay between human DNA repair proteins at a unique double-strand break in vivo. *EMBO J.*, **25**, 222–231.
19. Berkovich,E., Monnat,R.J. Jr. and Kastan,M.B. (2007) Roles of ATM and NBS1 in chromatin structure modulation and DNA double-strand break repair. *Nat. Cell Biol.*, **9**, 683–690.
20. Soutoglou,E., Dorn,J.F., Sengupta,K., Jasin,M., Nussenzweig,A., Ried,T., Danuser,G. and Misteli,T. (2007) Positional stability of single double-strand breaks in mammalian cells. *Nat. Cell Biol.*, **9**, 675–682.
21. Michaelis,C., Ciosk,R. and Nasmyth,K. (1997) Cohesins: chromosomal proteins that prevent premature separation of sister chromatids. *Cell*, **91**, 35–45.
22. Buerstedde,J.M. and Takeda,S. (1991) Increased ratio of targeted to random integration after transfection of chicken B cell lines. *Cell*, **67**, 179–188.
23. Takata,M., Sasaki,M.S., Sonoda,E., Morrison,C., Hashimoto,M., Utsumi,H., Yamaguchi-Iwai,Y., Shinohara,A. and Takeda,S. (1998) Homologous recombination and non-homologous end-joining pathways of DNA double-strand break repair have overlapping roles in the maintenance of chromosomal integrity in vertebrate cells. *EMBO J.*, **17**, 5497–5508.
24. Morrison,C., Sonoda,E., Takao,N., Shinohara,A., Yamamoto,K. and Takeda,S. (2000) The controlling role of ATM in homologous recombinational repair of DNA damage. *EMBO J.*, **19**, 463–471.
25. Sonoda,E., Zhao,G.Y., Kohzaki,M., Dhar,P.K., Kikuchi,K., Redon,C., Pilch,D.R., Bonner,W.M., Nakano,A., Watanabe,M. *et al.* (2007) Collaborative roles of gammaH2AX and the Rad51 paralog Xrcc3 in homologous recombinational repair. *DNA Repair (Amst)*, **6**, 280–292.
26. Dodson,H., Bourke,E., Jeffers,L.J., Vagnarelli,P., Sonoda,E., Takeda,S., Earnshaw,W.C., Merdes,A. and Morrison,C. (2004) Centrosome amplification induced by DNA damage occurs during a prolonged G2 phase and involves ATM. *EMBO J.*, **23**, 3864–3873.
27. Schultz,L.B., Chehab,N.H., Malikzay,A. and Halazonetis,T.D. (2000) p53 binding protein 1 (53BP1) is an early participant in the cellular response to DNA double-strand breaks. *J. Cell Biol.*, **151**, 1381–1390.
28. Jazayeri,A., Falck,J., Lukas,C., Bartek,J., Smith,G.C., Lukas,J. and Jackson,S.P. (2006) ATM- and cell cycle-dependent regulation of ATR in response to DNA double-strand breaks. *Nat. Cell Biol.*, **8**, 37–45.
29. Walker,M., Black,E.J., Oehler,V., Gillespie,D.A. and Scott,M.T. (2009) Chk1 C-terminal regulatory phosphorylation mediates checkpoint activation by de-repression of Chk1 catalytic activity. *Oncogene*, **28**, 2314–2323.
30. Paull,T.T., Rogakou,E.P., Yamazaki,V., Kirchgessner,C.U., Gellert,M. and Bonner,W.M. (2000) A critical role for histone H2AX in recruitment of repair factors to nuclear foci after DNA damage. *Curr. Biol.*, **10**, 886–895.
31. Sonoda,E., Matsusaka,T., Morrison,C., Vagnarelli,P., Hoshi,O., Ushiki,T., Nojima,K., Fukagawa,T., Waizenegger,I.C., Peters,J.M. *et al.* (2001) Scc1/Rad21/Mcd1 is required for sister chromatid cohesion and kinetochore function in vertebrate cells. *Dev. Cell*, **1**, 759–770.
32. Sjogren,C. and Nasmyth,K. (2001) Sister chromatid cohesion is required for postreplicative double-strand break repair in Saccharomyces cerevisiae. *Curr. Biol.*, **11**, 991–995.
33. Strom,L., Karlsson,C., Lindroos,H.B., Wedahl,S., Katou,Y., Shirahige,K. and Sjogren,C. (2007) Postreplicative formation of cohesion is required for repair and induced by a single DNA break. *Science*, **317**, 242–245.
34. Unal,E., Heidinger-Pauli,J.M. and Koshland,D. (2007) DNA double-strand breaks trigger genome-wide sister-chromatid cohesion through Eco1 (Ctf7). *Science*, **317**, 245–248.
35. Deckbar,D., Birraux,J., Krempler,A., Tchouandong,L., Beucher,A., Walker,S., Stiff,T., Jeggo,P. and Lobrich,M. (2007) Chromosome breakage after G2 checkpoint release. *J. Cell Biol.*, **176**, 749–755.
36. Heidinger-Pauli,J.M., Unal,E., Guacci,V. and Koshland,D. (2008) The kleisin subunit of cohesin dictates damage-induced cohesion. *Mol. Cell*, **31**, 47–56.
37. Kim,S.T., Xu,B. and Kastan,M.B. (2002) Involvement of the cohesin protein, Smc1, in Atm-dependent and independent responses to DNA damage. *Genes Dev.*, **16**, 560–570.
38. Yazdi,P.T., Wang,Y., Zhao,S., Patel,N., Lee,E.Y. and Qin,J. (2002) SMC1 is a downstream effector in the ATM/NBS1 branch of the human S-phase checkpoint. *Genes Dev.*, **16**, 571–582.
39. Rogakou,E.P., Pilch,D.R., Orr,A.H., Ivanova,V.S. and Bonner,W.M. (1998) DNA double-stranded breaks induce histone H2AX phosphorylation on serine 139. *J. Biol. Chem.*, **273**, 5858–5868.
40. Stiff,T., O'Driscoll,M., Rief,N., Iwabuchi,K., Lobrich,M. and Jeggo,P.A. (2004) ATM and DNA-PK function redundantly to phosphorylate H2AX after exposure to ionizing radiation. *Cancer Res.*, **64**, 2390–2396.
41. Burma,S., Chen,B.P., Murphy,M., Kurimasa,A. and Chen,D.J. (2001) ATM phosphorylates histone H2AX in response to DNA double-strand breaks. *J. Biol. Chem.*, **276**, 42462–42467.
42. Celeste,A., Fernandez-Capetillo,O., Kruhlak,M.J., Pilch,D.R., Staudt,D.W., Lee,A., Bonner,R.F., Bonner,W.M. and Nussenzweig,A. (2003) Histone H2AX phosphorylation is dispensable for the initial recognition of DNA breaks. *Nat. Cell Biol.*, **5**, 675–679.
43. Celeste,A., Petersen,S., Romanienko,P.J., Fernandez-Capetillo,O., Chen,H.T., Sedelnikova,O.A., Reina-San-Martin,B., Coppola,V., Meffre,E., Difilippantonio,M.J. *et al.* (2002) Genomic instability in mice lacking histone H2AX. *Science*, **296**, 922–927.